

LINEARITY, RESOLUTION, AND SYSTEMATIC ERRORS

*of the
CCD - RASNIK
Alignment System*

*Gerald Dicker, NIKHEF
May – July 1997*

Contents

1. ABSTRACT	2
2. THE EFFECTIVE PIXEL SIZE	2
2.1 Theory	2
2.2 Measurement.....	4
3. CCD AND MASK PITCH VARIATIONS	6
4. A FORMULA FOR THE Z-COORDINATE	7
5. LINEARITY AND ELECTRONICALLY LIMITED PERFORMANCE	8
5.1 Translations	9
5.2 Rotations	10
6. THE INFLUENCE OF THE LED CURRENT ON THE RESOLUTION	12
7. INHOMOGENEITY OF AIR TEMPERATURE	13
7.1 The Relationship between Air Temperature and Refractive Index... 13	
7.2 The Bending of Light Rays in a Constant Gradient Field..... 14	
7.3 The RASNIK Setup with a Constant Gradient Generator	15
7.4 Systematic Error Sources	19
7.5 Random Error Increasing Sources	22
7.6 Systematic Error Decreasing	22
7.7 Random Error Decreasing: Shielding	24
8. ERROR ANALYSIS	35
9. CONCLUSION	35
10. FILES INDEX	36

1. ABSTRACT

The RASNIK - ICARAS system is examined for linearity in the translation and rotation coordinates. A method for measuring the effective pixel size and the distance between ccd diode array and protection glass is presented. Resolution limiting caused by ccd / mask pitch variations, low LED current, and air temperature gradients is discussed. Formulae for the influence of a constant air temperature gradient on systematic measurement errors are derived and experimental verification is given. Shielding experiments have been carried out to study and improve the system's performance in a heat dissipating environment.

2. THE EFFECTIVE PIXEL SIZE

2.1 Theory

In general the effective pixel size of the ccd – frame grabber system is different from the physical pixel size of the ccd array since the ccd camera delivers an asynchronous signal to the frame grabber. Synchronization only exists for the y-coordinate because the signal is sent line by line. Fast frame grabbers improve resolution in the x direction yielding an effective pixel size which may be smaller than the actual physical pixel size. Fig.1 depicts the principle of measuring the effective pixel size. A piece of a RASNIK mask is glued on the protection glass of the ccd array and illuminated by a point shape light source. The arrow stands for one square of the mask. By making the distance (d) of the light source infinitely large in a gedankenexperiment, the magnification (M_{∞}) should equal one if the effective pixel size is chosen correct. From the deviation of M_{∞} from 1, we can calculate the correct effective pixel size.

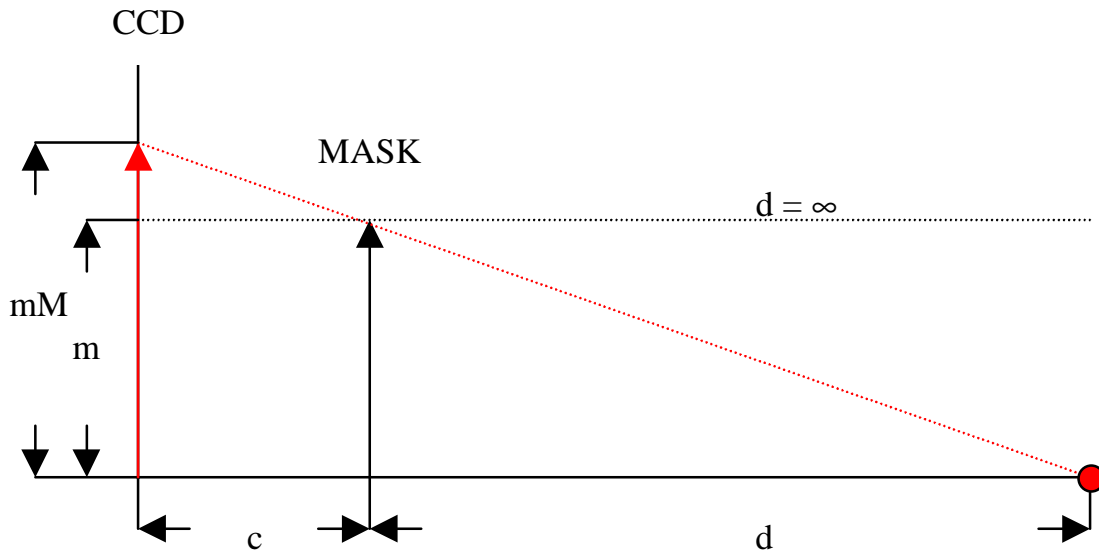


Fig. 1: Principle of measuring the effective pixel size with mask glued on ccd.

c...distance between mask and ccd array (= spacing between protection glass and diode array)

d...distance between mask and light source

m...mask pitch

M...magnification

mM...image mask pitch

From fig.1 we see:

$$\frac{d+c}{Mm} = \frac{d}{m} \quad (1)$$

yielding:

$$M = 1 + \frac{c}{d} \quad (2)$$

The magnification (M_m) measured by the ICARAS software is:

$$M_m = M \frac{p_{ass}}{p} \quad (3)$$

where:

p_{ass} ...assumed pixel size

p...correct effective pixel size

Letting d approach infinity, equ.3 becomes:

$$M_m(d = \infty) = M_\infty = \frac{p_{\text{ass}}}{p} \quad (4)$$

$$p = \frac{p_{\text{ass}}}{M_\infty} \quad (5)$$

Equ.3 multiplied with d gives a linear function in d.

$$M_m d = M_\infty d + c M_\infty \quad (6)$$

If $(M_m d)$ is plotted versus d, a linear fit will reveal M_∞ as the slope and $(c M_\infty)$ as the intercept of this curve.

$$c = \frac{\text{int ercept}}{M_\infty} \quad (7)$$

The effective pixel size can be calculated via equ.5.

2.2 Measurement

Tab. 1: Measurement series for determining the effective pixel size (p) and the distance (c) between ccd array and protection glass.

Camera...CHIPER CPT-8933

frame grabber...DATA TRANSLATION 3152

mask...RASNIK 120 microns

d...distance to the light source (source diameter: 1 cm)

M_m ...measured magnification

p_{ass} ...assumed pixel size (**6.298 μm**)

d / m :	1.00	1.50	2.00	3.00	6.0
+/- Δ d / m :	0.01	0.01	0.02	0.02	0.1
M_m :	1.001247	1.000704	1.000595	1.000297	1.000008
	1.001263	1.000711	1.000591	1.000296	1.000033
	1.001271	1.000726	1.000586	1.000312	1.000008
	1.001265	1.000712	1.000592	1.000274	0.999955
	1.001255	1.000702	1.000589	1.000293	0.999954
	1.001234	1.000709	1.000582	1.000308	0.999953
	1.001238	1.000730	1.000577	1.000300	0.999924
	1.001234	1.000745	1.000588	1.000285	0.999972

	1.001230	1.000726	1.000586	1.000275	0.999829
	1.001221	1.000704	1.000582	1.000292	1.000013
average :	1.001246	1.000717	1.000587	1.000293	0.999965
rms :	0.000017	0.000014	0.000005	0.000013	0.000059
$M_m d / m :$	1.001	1.501	2.001	3.001	6.00
$\pm \Delta (M_m d) / m :$	0.010	0.010	0.020	0.020	0.10

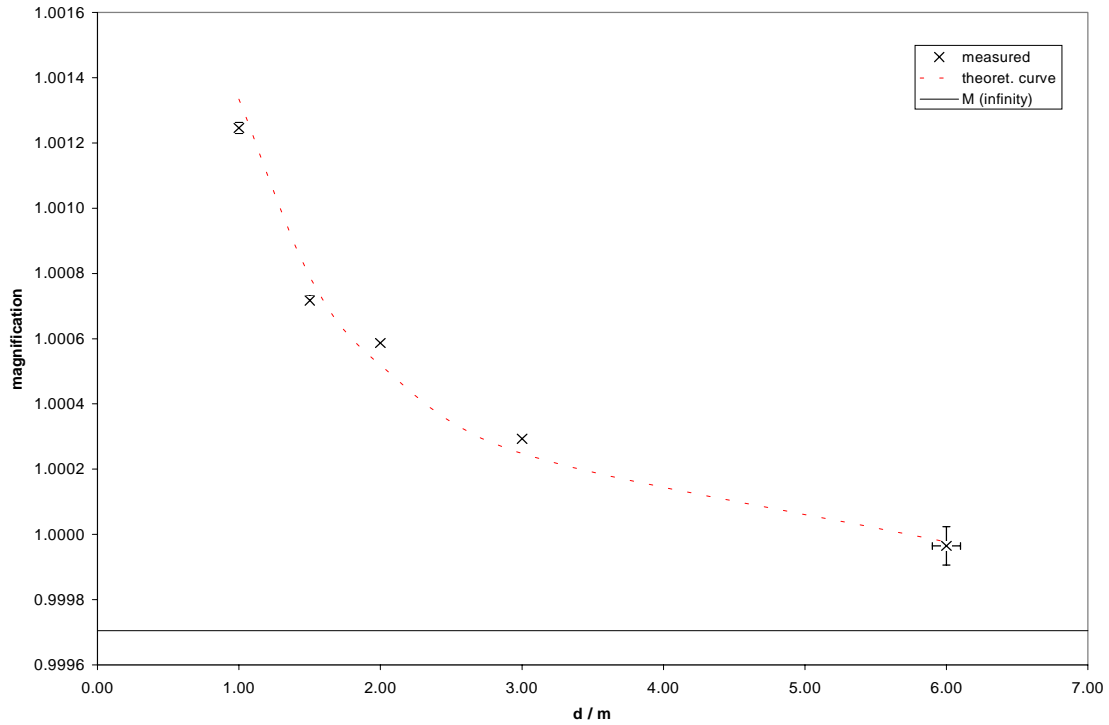


Fig. 2: The measured magnification (M_m) versus the distance (d) of the light source. The horizontal line represents the magnification for $d = \infty$ which is gained from the next plot (linear fit). Values from tab.1.

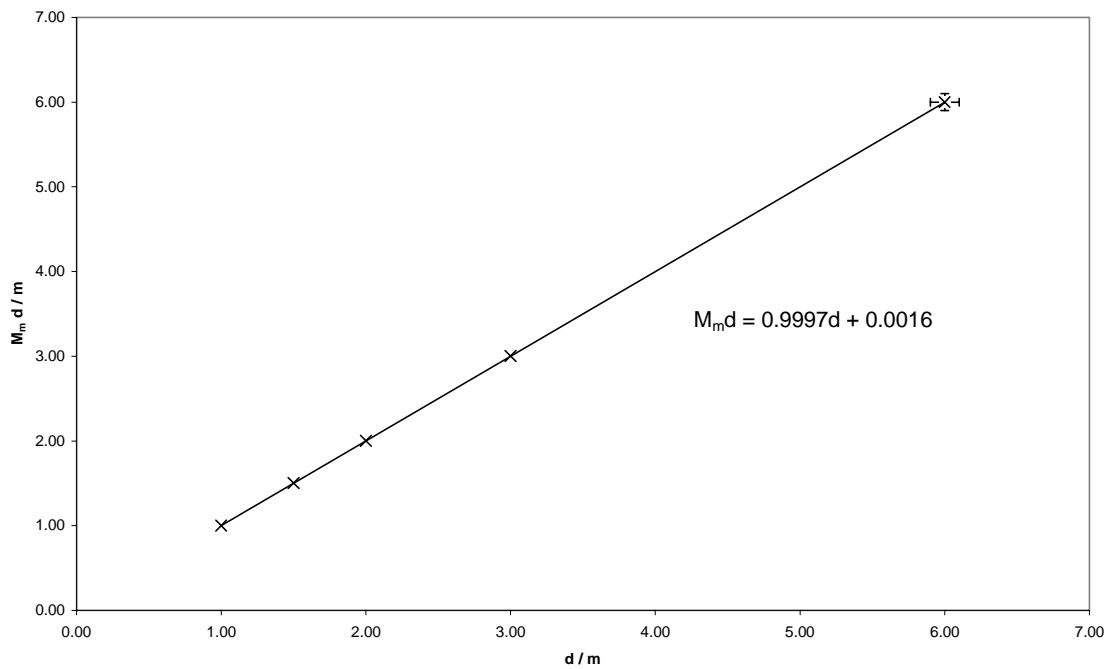


Fig. 3: Least squares linear fit for gaining the effective pixel size. Values from tab.1. Slope: 0.99971 ± 0.00004 , intercept: (1.63 ± 0.12) mm

The effective pixel size: **$p = (6.2999 \pm 0.0003) \mu\text{m}$**

The spacing: **$c = (1.63 \pm 0.12)$ mm**

3. CCD AND MASK PITCH VARIATIONS

Blocking different parts of the illuminating light beam for the same setup as in tab.1 (light source distance: 6m), reveals relative magnification changes of up to $2 \cdot 10^{-3}$ (for the y-coordinate). This value has been obtained by blocking 60% (from top to bottom) of the illuminated area leaving a rectangle of 1.2 mm x 4.5 mm free at the bottom. This is also the limit for the analysis program to work.

In order to be sure that this deviation is caused by varying ccd photo diode spacing, another experiment for measuring the mask pitch variation has been carried out. Using a small RASNIK setup ($f = 6.5$ cm, $M = 1$) the mask is slid over a 3 screw support to ensure that it moves in a fixed plane in space. When viewing different regions of the mask (by moving it in this defined plane), magnification changes measured by the ICARAS program must now be due to mask pitch variations. In the y-direction the maximum relative change of magnification is smaller than $2.5 \cdot 10^{-3}$ along the full mask height of

20 mm, i.e. a variation of $1.5 \cdot 10^{-4}$ within 1.2 mm which is (almost) negligible compared to $2 \cdot 10^{-3}$. In other words, the magnification changes measured above are due to ccd diode size (or spacing) variations. Hence, the mask pitch variation measured in the y direction is ± 0.3 microns. The maximum relative change of magnification in x measured is $5.6 \cdot 10^{-4}$ yielding a mask pitch variation of ± 0.07 microns.

The ccd errors do not significantly influence the measurements of x, y, and rot z when the whole array is illuminated. The case is different for the out of plane rotations rot x and rot y where errors will occur.

4. A FORMULA FOR THE Z-COORDINATE

In the following equations the distance between ccd and lens (= b) is assumed to be constant. The calculations refer to displacements of the mask. The distance between mask and lens (= g) is:

$$g = \frac{b}{M} \quad (8)$$

where M is the magnification.

A conventional definition of the z-coordinate assigns $z = 0$ to the situation where the imaging equation is fulfilled,

$$\frac{1}{f} = \frac{1}{b} + \frac{1}{g_0} \quad (9)$$

where f is the focal length. With the usual sign convention we get:

$$z = g_0 - g = g_0 - \frac{b}{M} \quad (10)$$

It is not easy to measure b with micron precision. An alternative formulation for the z-coordinate, which does not require a measurement of b but a sharp image on the screen, can be obtained as follows.

$$z = b \left(\frac{1}{M_0} - \frac{1}{M} \right) \quad (11)$$

$$b = f(M_0 + 1) \quad (12)$$

$$z = f(M_0 + 1)\left(\frac{1}{M_0} - \frac{1}{M}\right) \quad (13)$$

M_0 refers to the initial situation where the imaging equation is fulfilled (= sharp image).

5. LINEARITY AND ELECTRONICALLY LIMITED PERFORMANCE

Due to a damage of the frame grabber (DATA TRANSLATION 3152) it has had to be exchanged. The effective pixel size of the “new” one (MATRIX VISION, PC process M, MGVS module) in combination with the ccd camera (CHIPER CPT-8933) is measured to be:

$$p = (6.297 \pm 0.001) \mu\text{m}$$

A slightly different method than described above is employed for the measurement: The ccd, with the piece of mask glued on it, is illuminated by parallel light which has been produced by means of autocollimation.

In order to measure the ultimate i.e. electronically limited performance, a small setup (called “mini”) with a lens (MELLES GRIOT 01LDX125) of short focal length ($f = 63.5$ mm, $D = 40$ mm) is used. With a short light path through the air, temperature effects can practically be excluded. It has turned out that the spherical aberrations of the lens cause the image to turn gray and the ICARAS software to fail. As a consequence the lens diameter has been decreased to 20 mm by using a diaphragm of black paper reducing the influence of the wrong curvature of the outer lens region. The setup is used in the symmetrical ($M = 1$, $b = g = 2f$) situation. For producing well defined three dimensional displacements, a high-precision mount (NEWPORT M-460A) driven by three micrometer screws is used. Rotations are carried out with a rotating mount (M-TGN80). A uniform illumination of the mask is met by using nine infrared LEDs and a ground glass plate. In the following diagrams the errors of the RASNIK measured values are gained from the standard deviation of ten measurements. A least squares linear approximation yields the slope of the plotted trendlines.

5.1 Translations

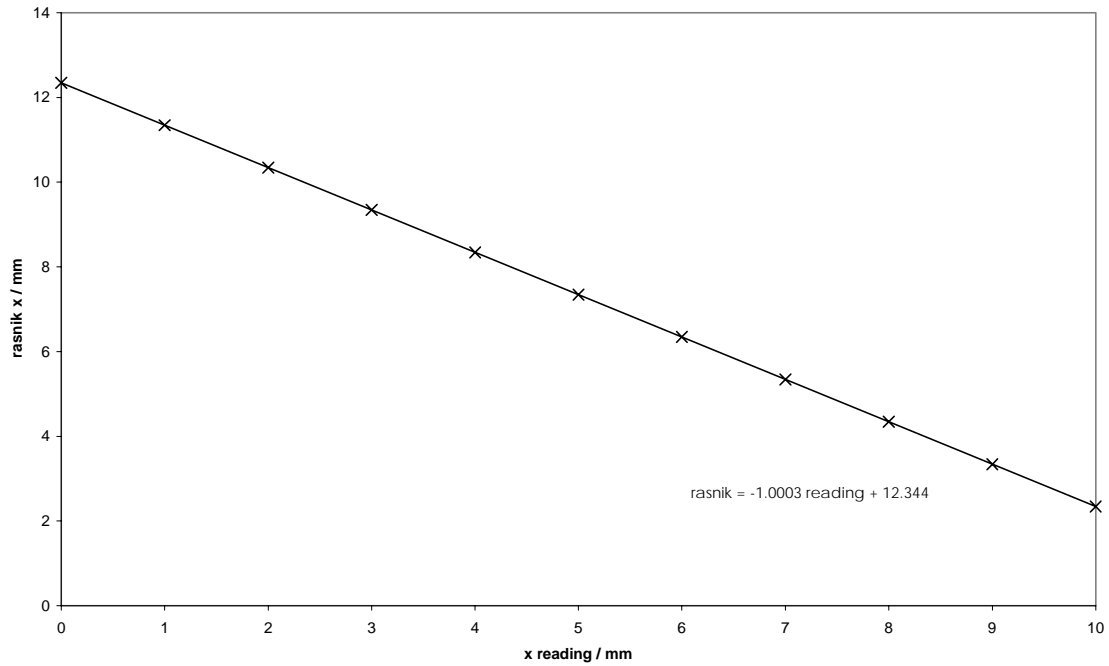


Fig. 4: The linearity of the x-coordinate. Slope = -1.00029 ± 0.00007 ,
 $\Delta x_{\text{reading}} = \pm 3 \mu\text{m}$, $\Delta x_{\text{RASNIK}} = \pm 0.1 \mu\text{m}$

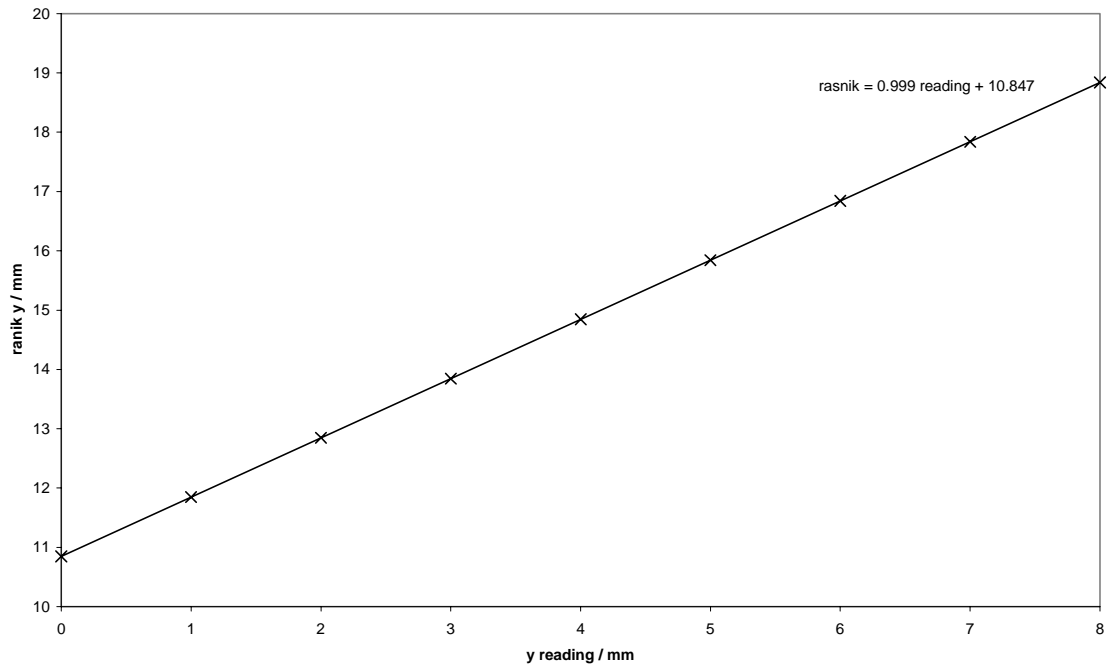


Fig. 5: The linearity of the y-coordinate. Slope = 0.9990 ± 0.0001 ,
 $\Delta y_{\text{reading}} = \pm 3 \mu\text{m}$, $\Delta y_{\text{RASNIK}} = \pm 0.1 \mu\text{m}$

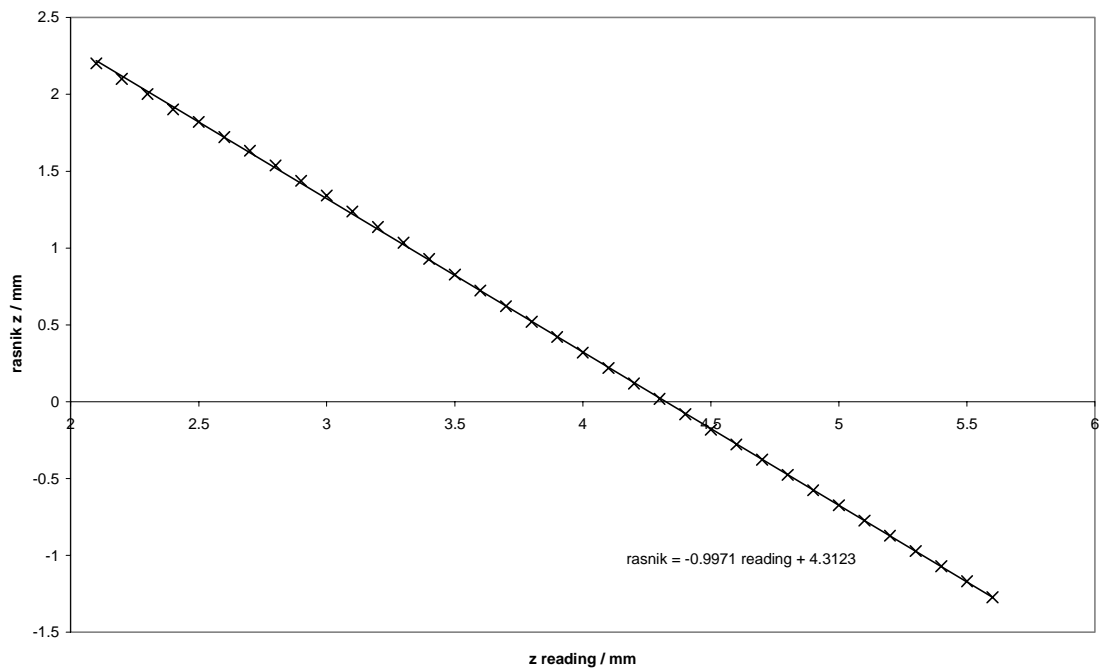


Fig. 6: The linearity of the z-coordinate. Slope = -0.9971 ± 0.0016 , $\Delta M_{\text{RASNIK}} = \pm 3 \cdot 10^{-5}$, $\Delta z_{\text{reading}} = \pm 3 \mu\text{m}$, $\Delta z_{\text{RASNIK}} = \pm 1 \text{ mm}$ (from the uncertainty of b and g_0). The z -value has been calculated from the magnification (M) via equ.10. Error bars are not shown since they only reflect the errors of b and g_0 .

5.2 Rotations

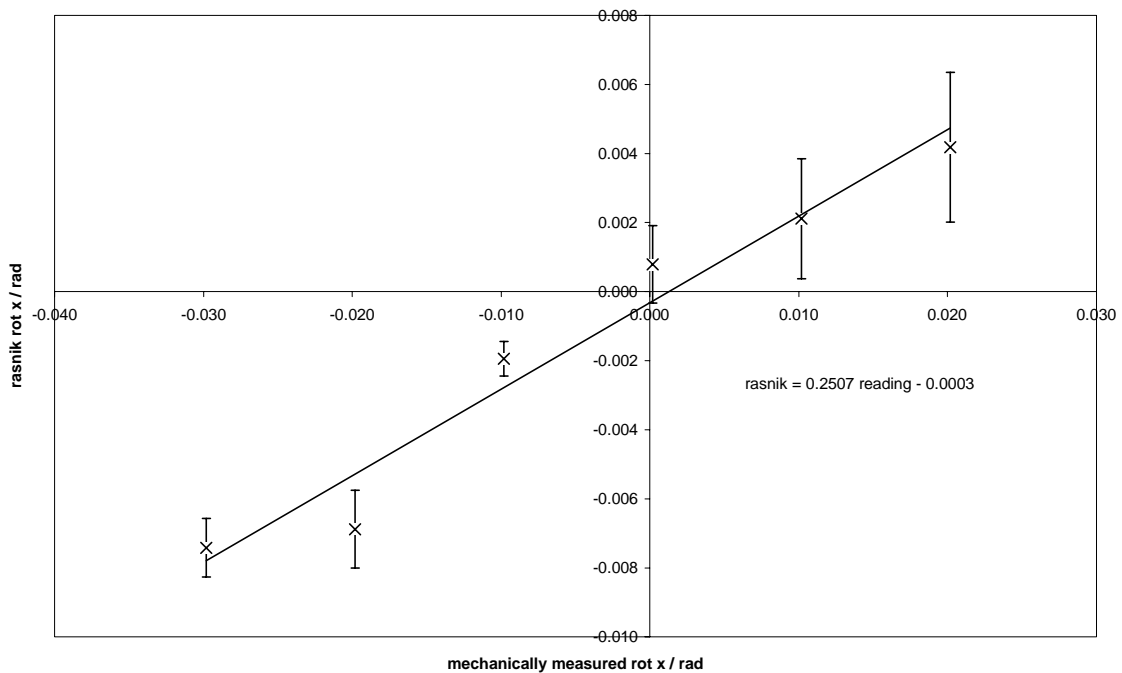


Fig. 7: The rotation around the x-axis. Slope = 0.25 (instead of 1).

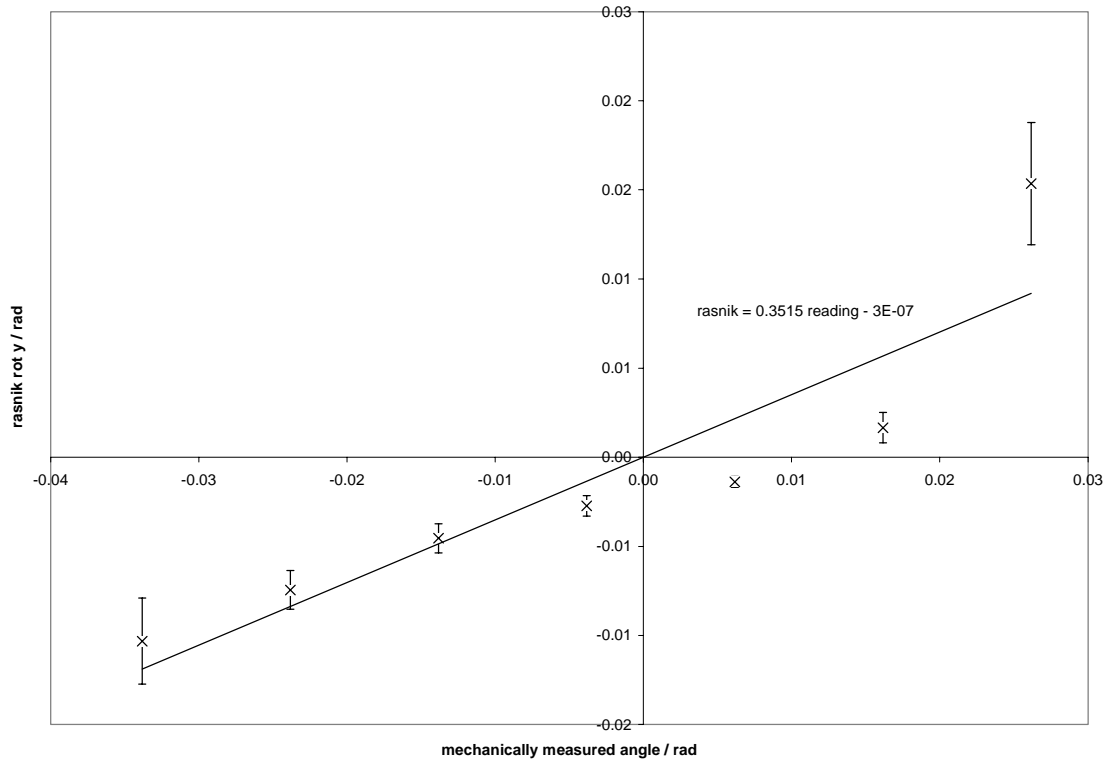


Fig. 8: The rotation around the y-axis. Slope = 0.35 (instead of 1).

Additional problems with measuring the out-of-plane rotations rot x and rot y might arise from the ccd pitch variations as stated in chapter 3.

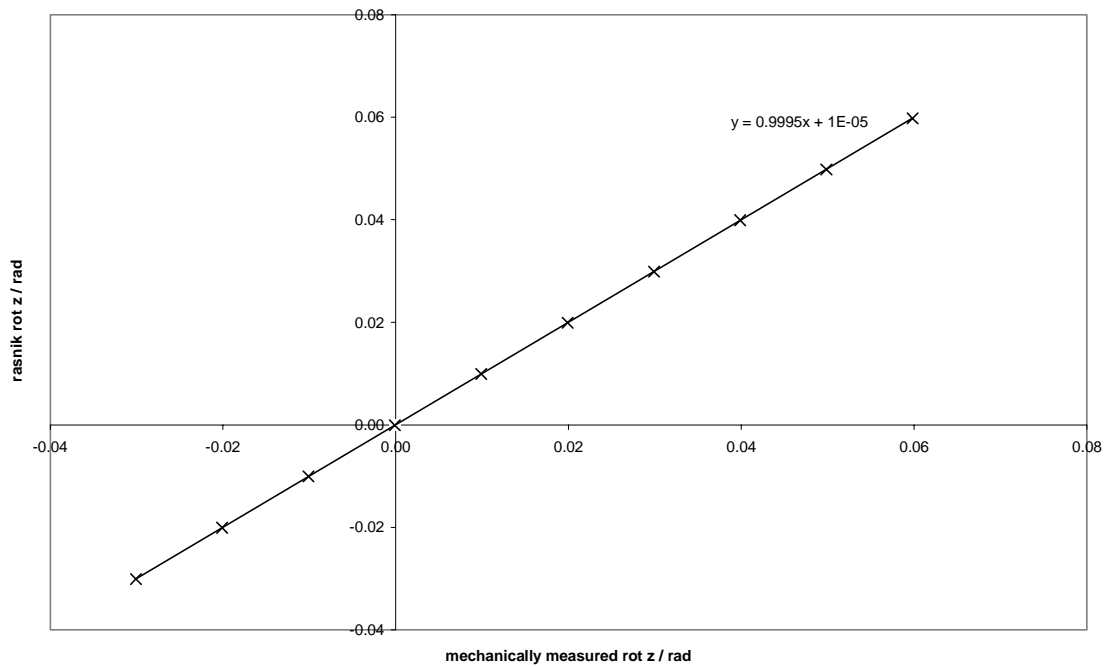


Fig. 9: The rotation around the z-axis. Slope = 0.9996 ± 0.0002 , $\Delta (\text{rot } z)_{\text{reading}} = 0.3 \text{ mrad}$, $\Delta (\text{rot } z)_{\text{RASNIK}} = 0.02 \text{ mrad}$

6. THE INFLUENCE OF THE LED CURRENT ON THE RESOLUTION

The same setup as before is used to study the influence of the current through the mask illuminating infrared diodes on the resolution. In order to make current changes possible, the two transistors which act as constant current sources are removed from the circuit board. One branch (4 LEDs) is left without power supply, the other one (5 LEDs) is connected to a 100 Ohm resistor and a digital ampere meter in series. Now a change of the input voltage (0-15 V) induces a change of the current through the five diodes. The mask area “seen” by the ccd is chosen to be in the region of the five working diodes. In principal all RASNIK coordinates behave like the magnification which is shown as a representative chart below.

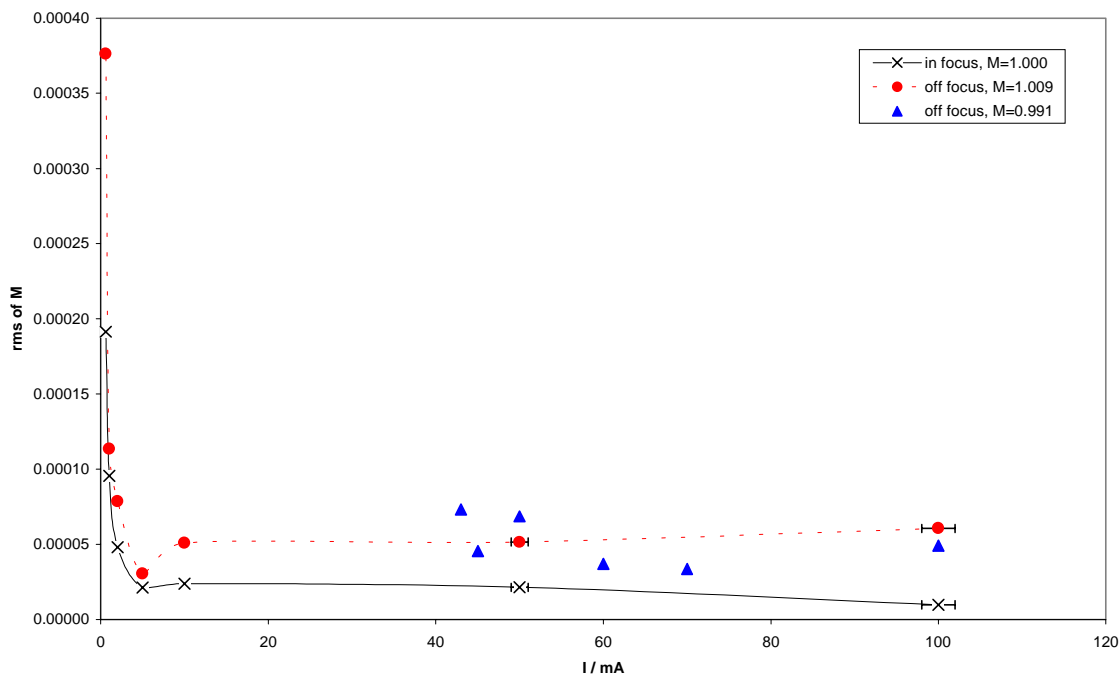


Fig. 10: The influence of the LED current (I) on the resolution of the magnification. RMS from ten measurements. The two off focal measurement series refer to the maximum z-displacements measurable by ICARAS for this setup. For $M = 0.991$ the minimum current necessary has been 43 mA.

From fig.10 one can see that no significant decline of the resolution for the in-focus situation is observable with currents down to 10 mA. Reliable operation in the full range is guaranteed from 60 mA. No stabilization of the current by

means of transistors is needed. In large setups a condenser lens replaces the ground glass plate to ensure uniform illumination.

7. INHOMOGENEITY OF AIR TEMPERATURE

7.1 The Relationship between Air Temperature and Refractive Index

An empirical formula for the dependence of the refractive index of air on the temperature at a pressure of 760 Torr and at a wavelength of 850 nm is used¹:

$$\Delta n_t = \frac{\Delta n_0}{1 + \alpha t} \quad (14)$$

with: $\Delta n_0 = 2895 \cdot 10^{-7}$

$$\alpha = 0.003672 \text{ (}^\circ\text{C)}^{-1}$$

where:

Δn_t ...the difference of the refractive index to vacuum

Δn_0 ...the difference of the refractive index to vacuum at $t = 0 \text{ }^\circ\text{C}$

t ...temperature in $^\circ\text{C}$

Expanding this expression into a power series around $t = 20 \text{ }^\circ\text{C}$ and neglecting higher order terms yields:

$$\Delta n_t \approx \frac{\Delta n_0}{1 + 20\alpha} - \frac{\Delta n_0 \alpha (t - 20)}{(1 + 20\alpha)^2} + O \quad (15)$$

With this linear expression one can easily calculate a constant gradient (K) between two points of different temperatures (t_t and t_b) separated by a distance h . The letters t , b , and h refer to top, bottom, and height, respectively, for reasons of clearness.

¹ Robert C. Weast (editor), Handbook of Chemistry and Physics, Chemical Rubber Publishing Company, 58th ed., p. E224

$$K = \frac{\Delta n_0 \alpha}{h(1 + 20\alpha)^2} (t_b - t_t) \quad (16)$$

7.2 The Bending of Light Rays in a Constant Gradient Field

In geometrical optics light propagating through a medium is described in terms of light rays. In a medium of homogeneous refractive index these rays are straight lines. The differential equation of light rays is given by²:

$$\frac{d}{ds} \left(n \frac{d\vec{r}}{ds} \right) = \vec{\nabla} n \quad (17)$$

where:

s ...length of the ray measured from a fixed point on it

\vec{r} ...position vector

n ...refractive index

We want to limit our considerations on two dimensions and furthermore make the following assumptions:

1. Constant gradient of the refractive index in the y direction: $\vec{\nabla} n := K \cdot \vec{e}_y$
2. The light ray initially travels parallel to the x-axis.
3. For "small" deviations of the light beam from the initial horizontal direction

we may assume $\frac{dn}{ds} \approx 0$, hence $n(s) = \bar{n}$.

We obtain the following system which is easily solved.

$$\frac{d^2 x}{ds^2} = 0 \quad (18)$$

$$\bar{n} \frac{d^2 y}{ds^2} = K \quad (19)$$

If the origin of the light ray and the one of our coordinate system coincide, we get the following trajectory in parametric form.

$$x = s \quad (20)$$

² Max Born and Emil Wolf, Principles of Optics, Pergamon Press, 6th ed., p.122

$$y = \frac{Ks^2}{2\bar{n}} \quad (21)$$

The result is a quadratic deviation from the straight line with the light ray bending towards the region of higher refractive index.

$$y(x) = \frac{Kx^2}{2\bar{n}} \quad (22)$$

7.3 The RASNIK Setup with a Constant Gradient Generator

7.3.1 Experimental Arrangement

For studying the air temperature influence, a large RASNIK setup (called “big”) with a total length of 7.18 meters is used. The mask pitch in this setup is 170 μm , the lens diameter (D) 45 mm. A constant gradient generator is realized as follows. An aluminum tube with rectangular cross section is heated with heating ropes at its top (see fig.11). Either end of the hollow bar is covered with a transparent foil to minimize air convection. There are two principal arrangements for testing the influence of a constant gradient generator on the RASNIK system. The generator can be placed either between lens and ccd (fig.12) or between mask and lens (fig.13).

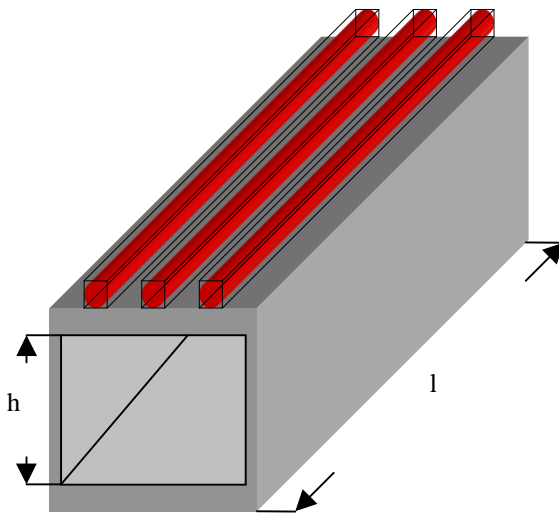


Fig. 11: The constant gradient generator.

$h = (100 \pm 1) \text{ mm}$, $l = (1000 \pm 1) \text{ mm}$.

For the calculations to come, the values of g , b , f , a , and l are always taken to be positive. In order to get the displacement of the image in the first case, we calculate the tangent of the light path at $x = l$ (see fig.12) by differentiating equ.22.

$$\left(\frac{dy}{dx}\right)_l = \frac{Kl}{\bar{n}} \quad (23)$$

The intercept of this tangent is $-\frac{Kl^2}{2\bar{n}}$ yielding the straight line equation.

$$y_t = \frac{Kl}{2\bar{n}}(2x - l) \quad (24)$$

With $x = b - a$ this equation becomes:

$$\Delta y = \frac{Kl}{2\bar{n}}[2(b - a) - l] \quad (25)$$

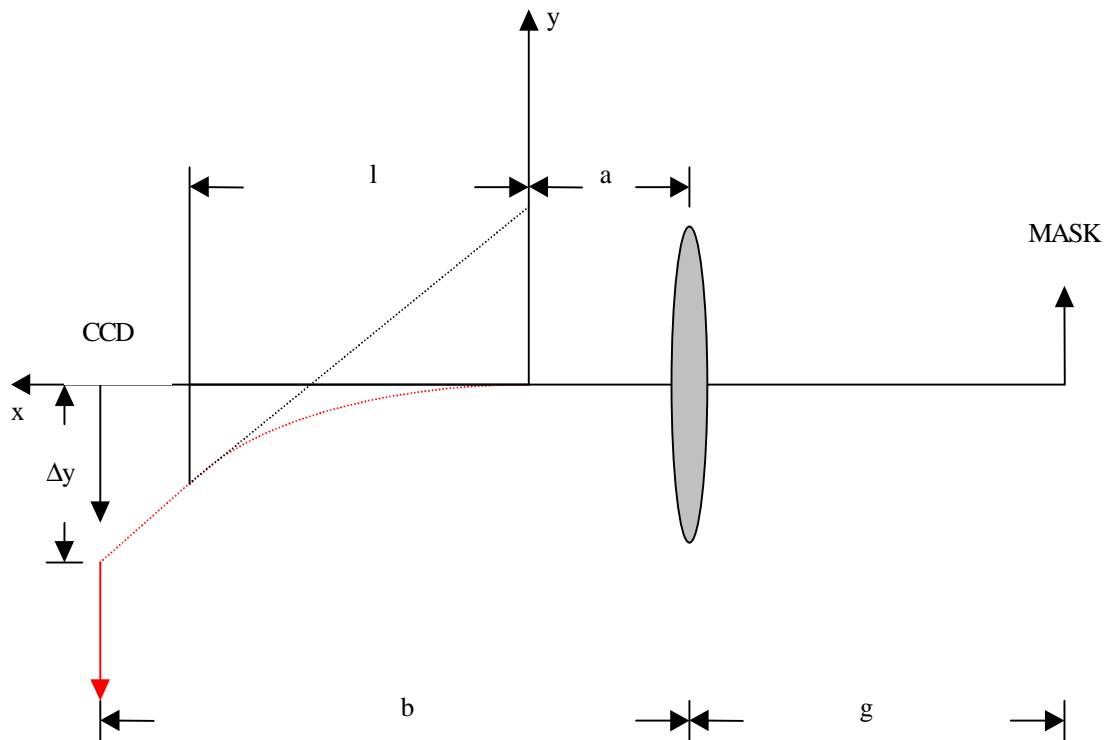


Fig. 12: The gradient generator between lens and ccd.

l ...length of the tube

g ...distance lens – mask

b ...distance ccd – lens

7.3.2 Measurements

The Rasnik y value is measured after heating the tube for at least 20 minutes when a stable gradient is achieved. The value measured before heating is then subtracted from it. The error is gained by the rms of ten consecutive measurements taking the subtraction into account. The temperatures are measured with sensors wrapped round with aluminum foil and glued on the bar with a sticky tape. The top temperature is measured by three digital sensors distributed on the roof, the bottom one with two sensors (one did not work properly). The measurement error of one sensor is indicated to be ± 1 °C.

Tab. 2: Theoretical and measured image displacements.

arr...arrangement (1...see fig.12, 2...see fig.13)

a...distance between lens and gradient generator

t_t (t_b)...temperature at the top (bottom) of the tube (measured with sensors)

\bar{n} ...average refractive index

K...refractive index gradient

M...magnification

Δy_t (Δy_m)...calculated (measured) image displacement

arr	a / mm	$\pm \Delta a$ / mm	t_t / °C	t_b / °C	\bar{n}	$\pm \Delta \bar{n}$	K / (mm) ⁻¹	$\pm \Delta K$ / (mm) ⁻¹	Δy_t / μm	M	Δy_m / μm
1	550	2	45.6	37.1	1.0002513	6E-7	-7.8E-08	1.4E-08	-234 ± 42	1.2829	-199 ± 5
1	1800	10	48.4	40.4	1.0002489	6E-7	-7.4E-08	1.4E-08	-128 ± 25	1.2847	-111 ± 3
2	225	2	54.7	45.5	1.0002445	5E-7	-8.5E-08	1.4E-08	-265 ± 46	1.2824	-221 ± 6
2	1600	5	47.7	41.5	1.0002488	5E-7	-5.7E-08	1.3E-08	-77 ± 20	1.2798	-63 ± 10

Errors of measured quantities:

$$\Delta t = \pm 0.7 \text{ °C}$$

Formulae:

$$\Delta y_m = \Delta y_{\text{RASNIK}} \cdot M^3$$

K...equ.16

Δy_t ...equ.25,28

$$\bar{n} = 1 + \frac{\Delta n_0}{1 + \alpha t} \quad (29)$$

$$t = (t_t + t_b) / 2 \quad (30)$$

with:

$$f = 1774 \text{ mm} \quad g = (3150 \pm 10) \text{ mm}$$

$$b = (4030 \pm 10) \text{ mm} \quad h = (100 \pm 1) \text{ mm}$$

$$l = (1000 \pm 1) \text{ mm} \quad \Delta n_0, \alpha \dots \text{see equ.14}$$

The systematic deviations of the measured image displacements from the theoretically predicted ones in tab.2 are all within the error tolerance. However, they are 16 % lower on average which may be interpreted as systematic. This indicates that the gradient is not constant as assumed or about 16 % systematically lower than calculated. From shielding experiments the former assumption seems quite appropriate for one can see there that the vertical gradient within a common shield, i.e. a shield with top, bottom, and side shields, is larger close to the top and smaller close to the bottom of the shield. The light beam in this experiment has passed the gradient generator close to the bottom.

7.4 Systematic Error Sources

Heat sources close above the light beam mainly induce systematic errors whereas heating below the axis merely induces an increase of the random error. In the latter case one might expect an upward bending of light rays. This

³ The measured RASNIK value Δy_{RASNIK} has to be multiplied with the magnification (M) because the ICARAS software gives the displacement in terms of the mask displacement but not the actual displacement of the image.

is not the case since the generation of a stable temperature gradient is always disturbed by the ascent of warm air from the heat source below yielding a blurring of the image (high random error) rather than a systematical displacement. The influence of the gradient on the image displacement is linear with its distance from the ccd or the mask, respectively (see equs.25, 28, and figs.12, 13). The closer the heat source is to the lens the larger errors occur. In the following plots the systematic error is obtained through averaging over ten consecutive measurements and subtracting this value from the averaged value of ten measurements without heating (negative time). In order to measure a reliable random error (= standard deviation of ten consecutive measurements) the heat capacity of the studied sources has to be large enough, so that the temperature within ten measurements (for obtaining the random error) can be assumed constant.

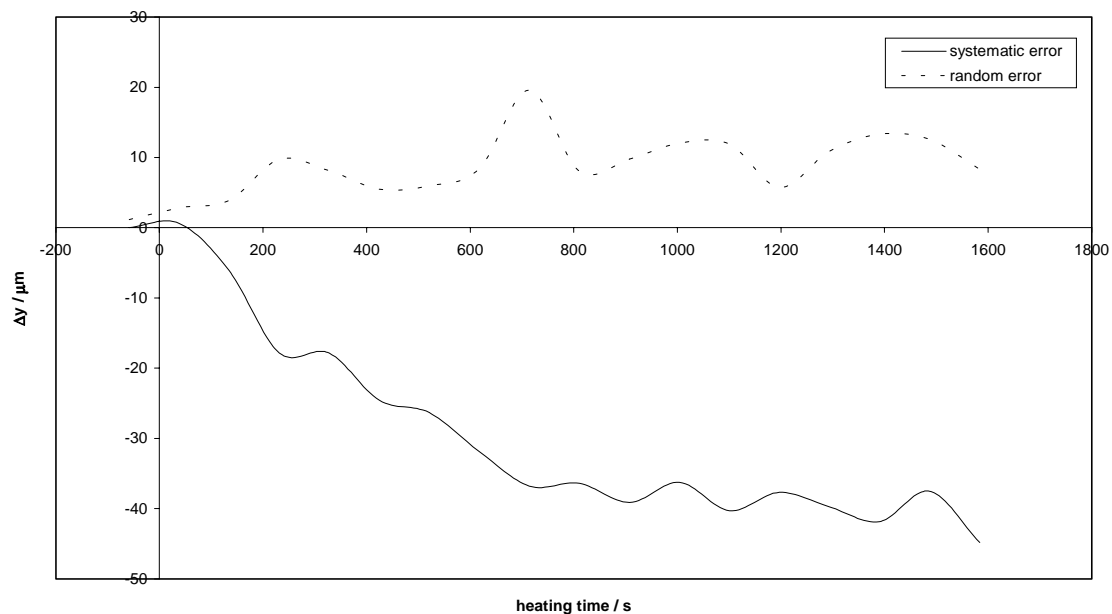


Fig. 14: Aluminum sheet as systematic error source. The sheet (thickness: 1.5 mm) is heated with a heating rope lying on it and is placed close (3 cm) above the optical axis. The distance of one edge to the lens is about 20 cm and the light beam is influenced on a length of 59 cm.

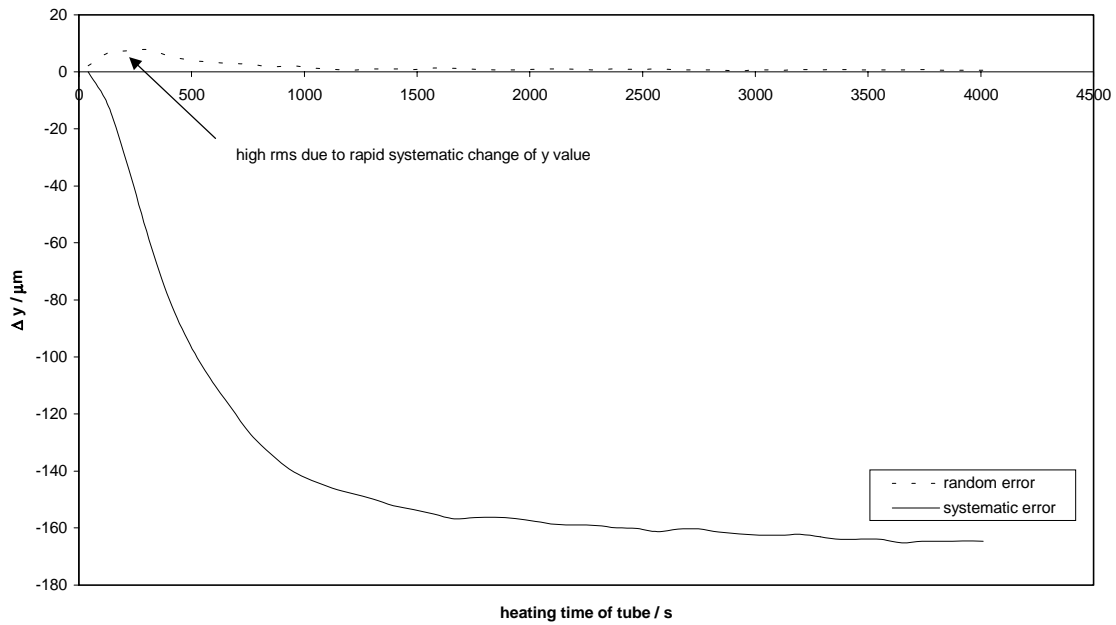


Fig. 15: The constant gradient generator (between lens and ccd) as a systematic error source.

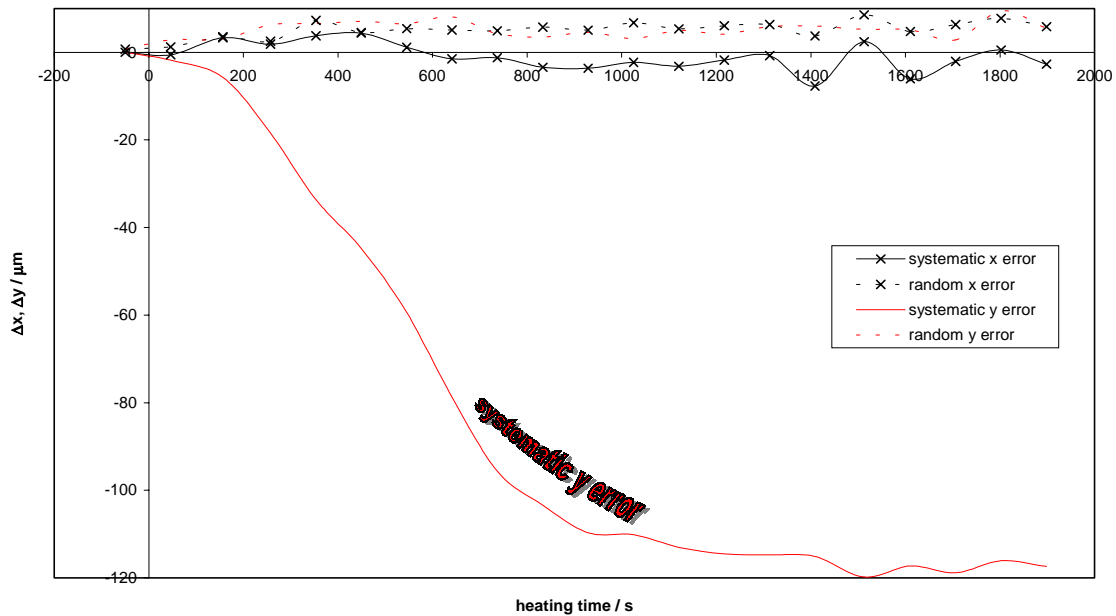


Fig. 16: The constant gradient generator rotated by 90 degrees. Instead of expecting a larger shift in x than in y, the opposite is true. This fact indicates that if common shielding is applied for reducing the random error, a systematic error in y will probably result (see the chapter on shielding).

7.5 Random Error Increasing Sources

In the experiments carried out no systematic error has been observed when placing a heat source below the light beam. Fig.17 serves as an example for random error increase.

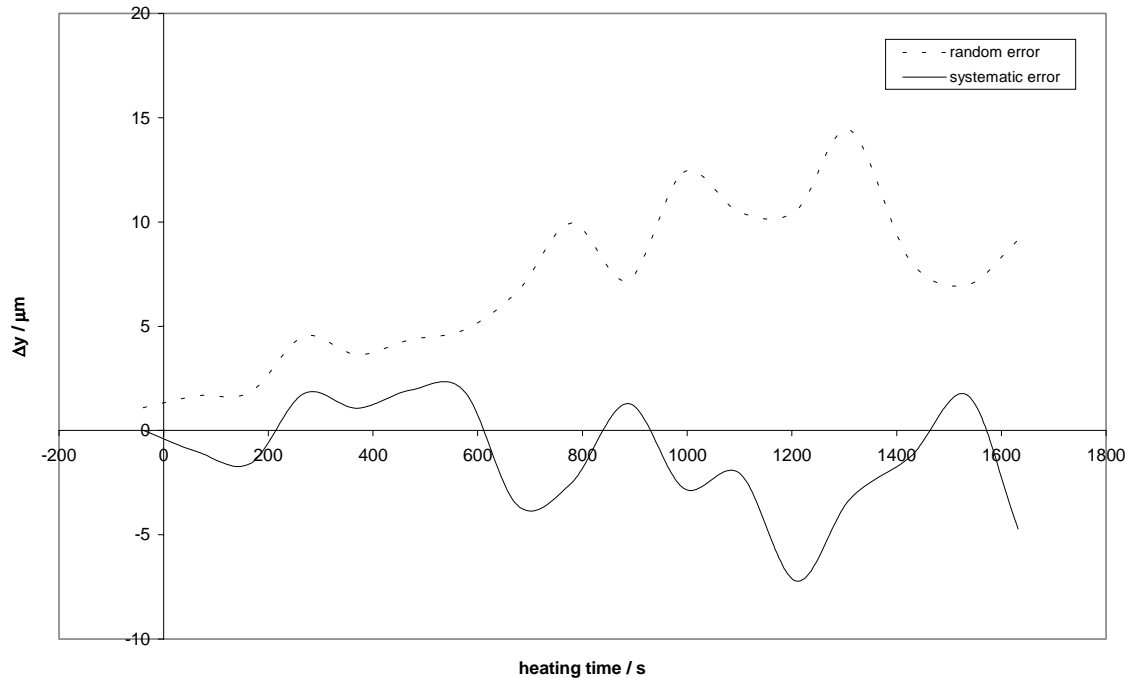


Fig. 17: Aluminum box filled with a heating rope as a random error increasing source. The heat source is placed about 1 m below the axis and 1.5 m away from the lens. Box dimensions: 23 x 20 x 10 cm³, 3 mm thick body.

7.6 Systematic Error Decreasing

In all the following experiments the same heat source as mentioned in Fig.17 has been used. In order to reduce systematic errors one has to take care that the medium (air) the beam passes through is in random movement. This can be achieved e.g. through circulating the air by means of ventilators. As will be seen later, shields of the common type (with top, bottom, and side shields) may cause systematic errors which can be reduced by blowing air through them. Fig.18 depicts an example of systematic error decrease by applying the latter technique.

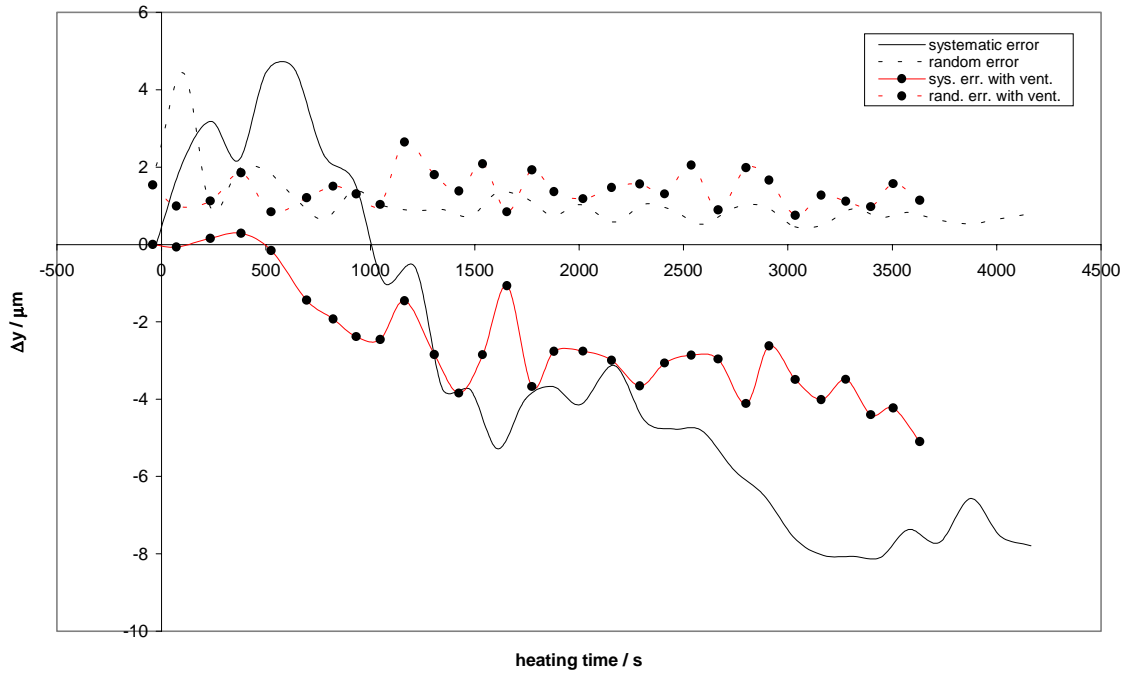


Fig. 18: Systematic error decreasing by means of blowing air through a shield (round alu pipe, diameter: 11 cm, length: 239 cm).

However, this technique has not helped decrease the systematic error in x which can be seen from the next plot.

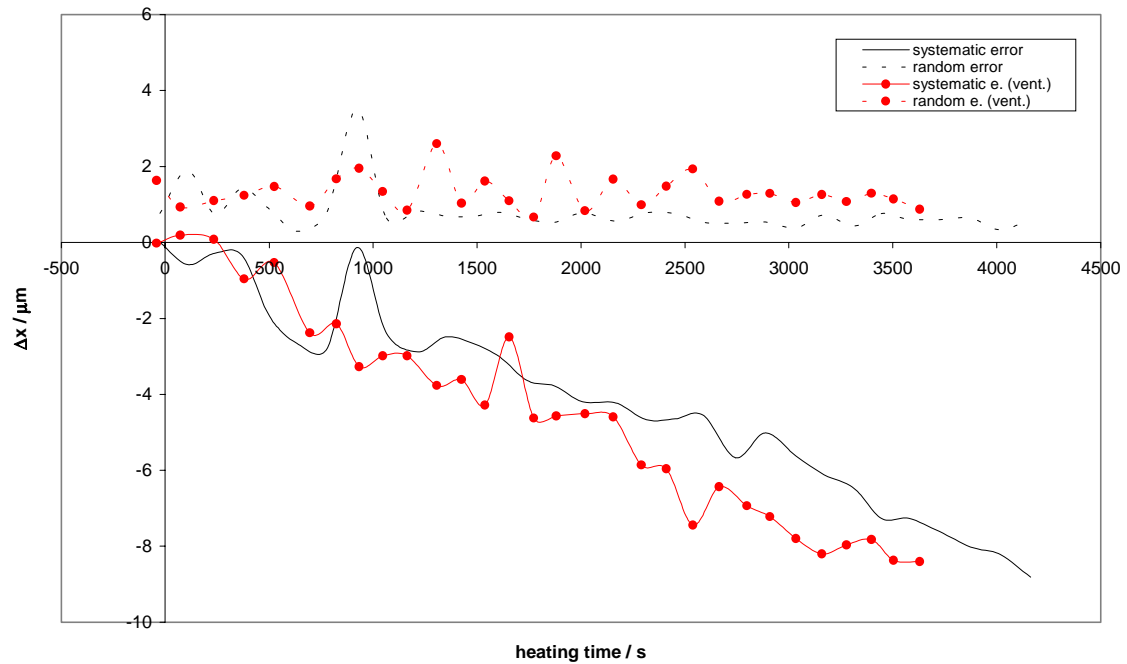


Fig. 19: The systematic error in the x-coordinate for the same setup as in fig.18.

7.7 Random Error Decreasing: Shielding

Whenever large fluctuations of the refractive index due to a heat source below the optical axis occur, shielding of the beam is required to minimize random errors. In the following chapters a round aluminum pipe as mentioned above and a shield, also made of aluminum, with a cross section of the shape of an isosceles triangle with a right angle are used. The baseline of this triangle is 26.5 cm and the thickness of the sheets is 1 mm. The shield is 150 cm long. The triangular shield is used in two different ways. It is used with the baseline on the bottom (Δ , upright) or turned around by 180° resembling a “give way” – traffic sign (∇ , gws). Each setup is tested with the light beam passing near the top and the bottom of the shield. In order to evaluate the absolute effectiveness of each shield, the deviations of the Rasnik values when no shielding is applied are depicted in the chapter: *The Flat Sheet*.

7.7.1 The X-Coordinate

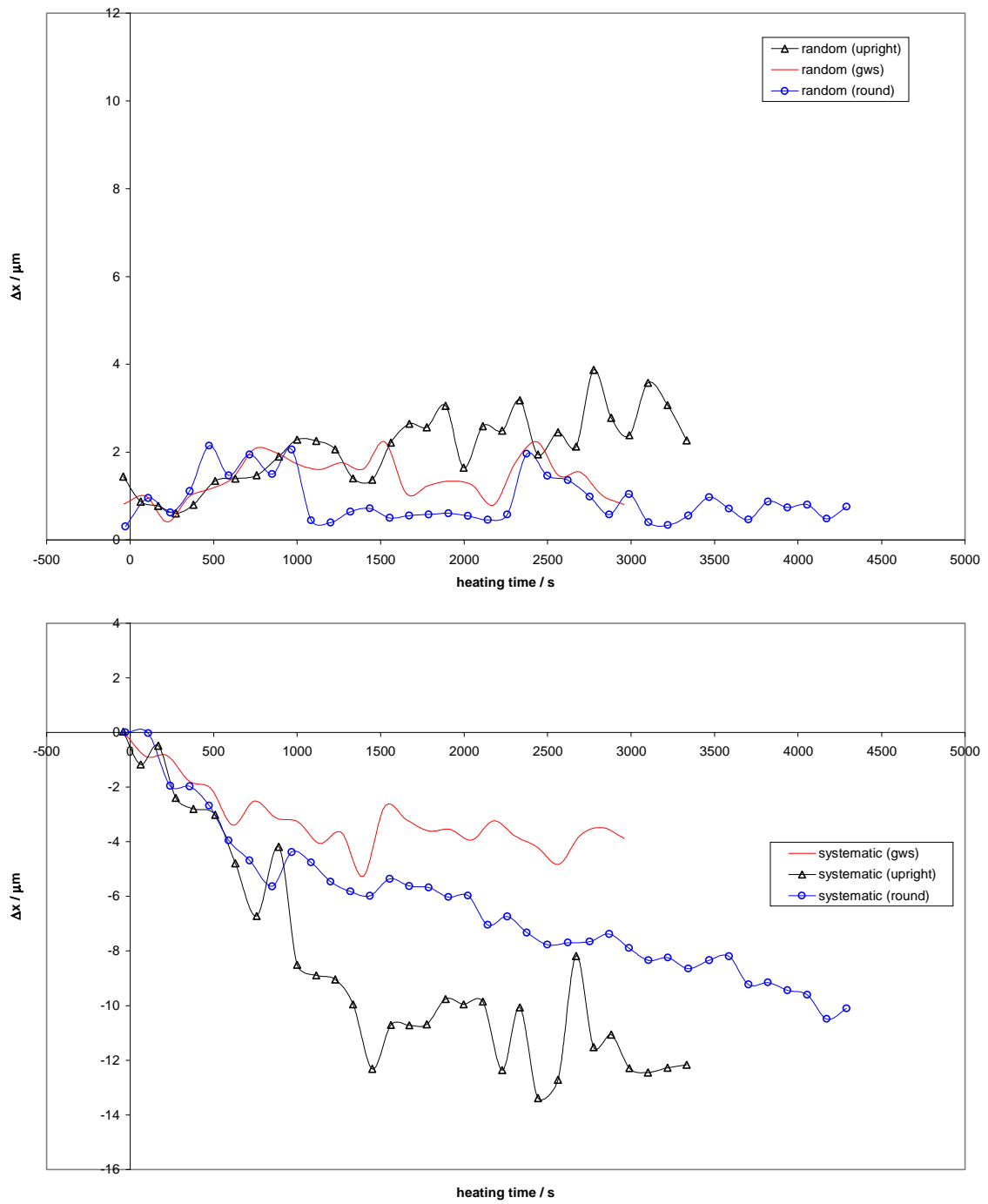


Fig. 20: Random and systematic errors with different shields. Beam passes at the top.

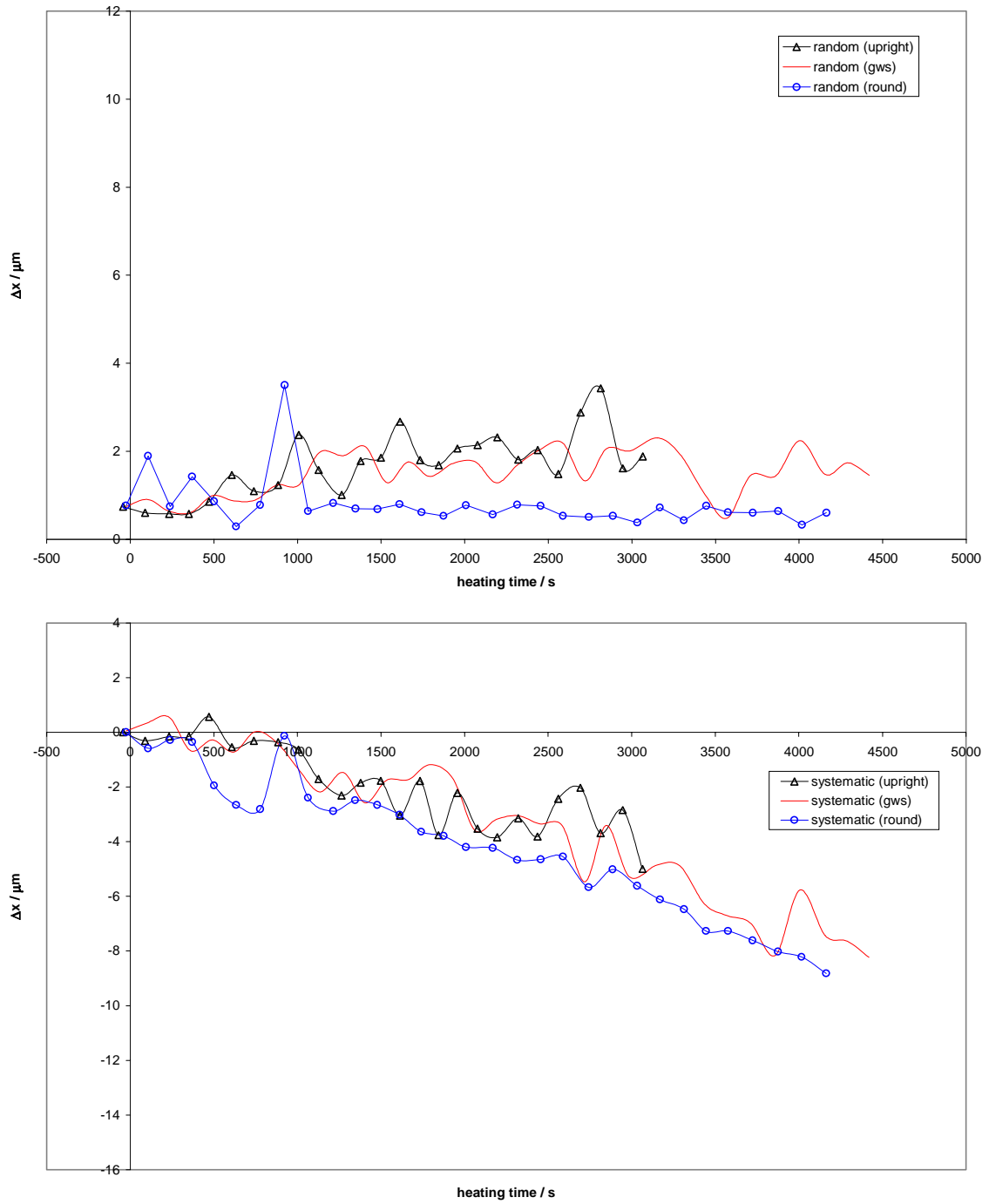


Fig. 21: Random and systematic errors with different shields. Beam passes at the bottom.

7.7.2 The Y-Coordinate

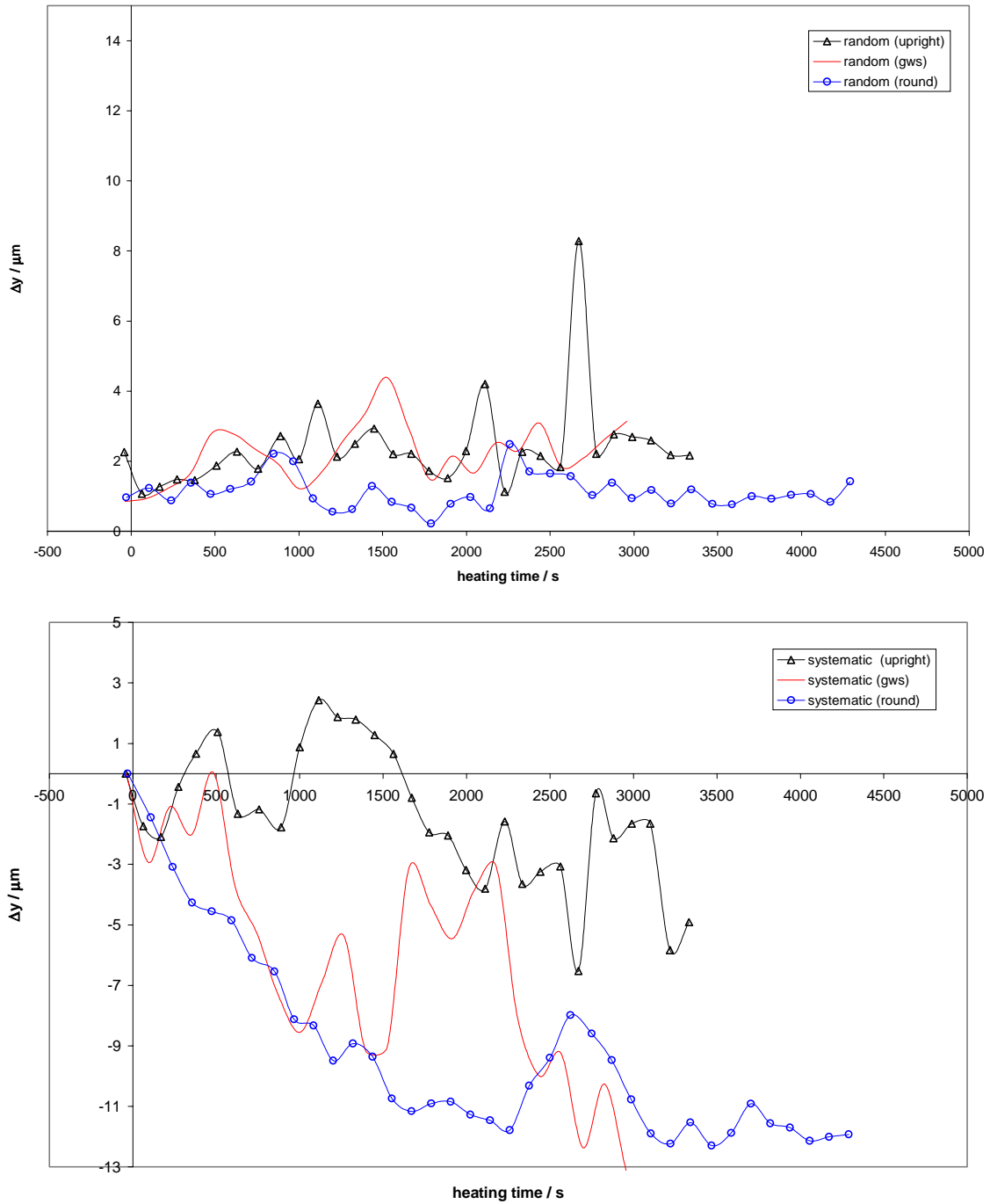


Fig. 22: Random and systematic errors with different shields. Beam passes at the top.

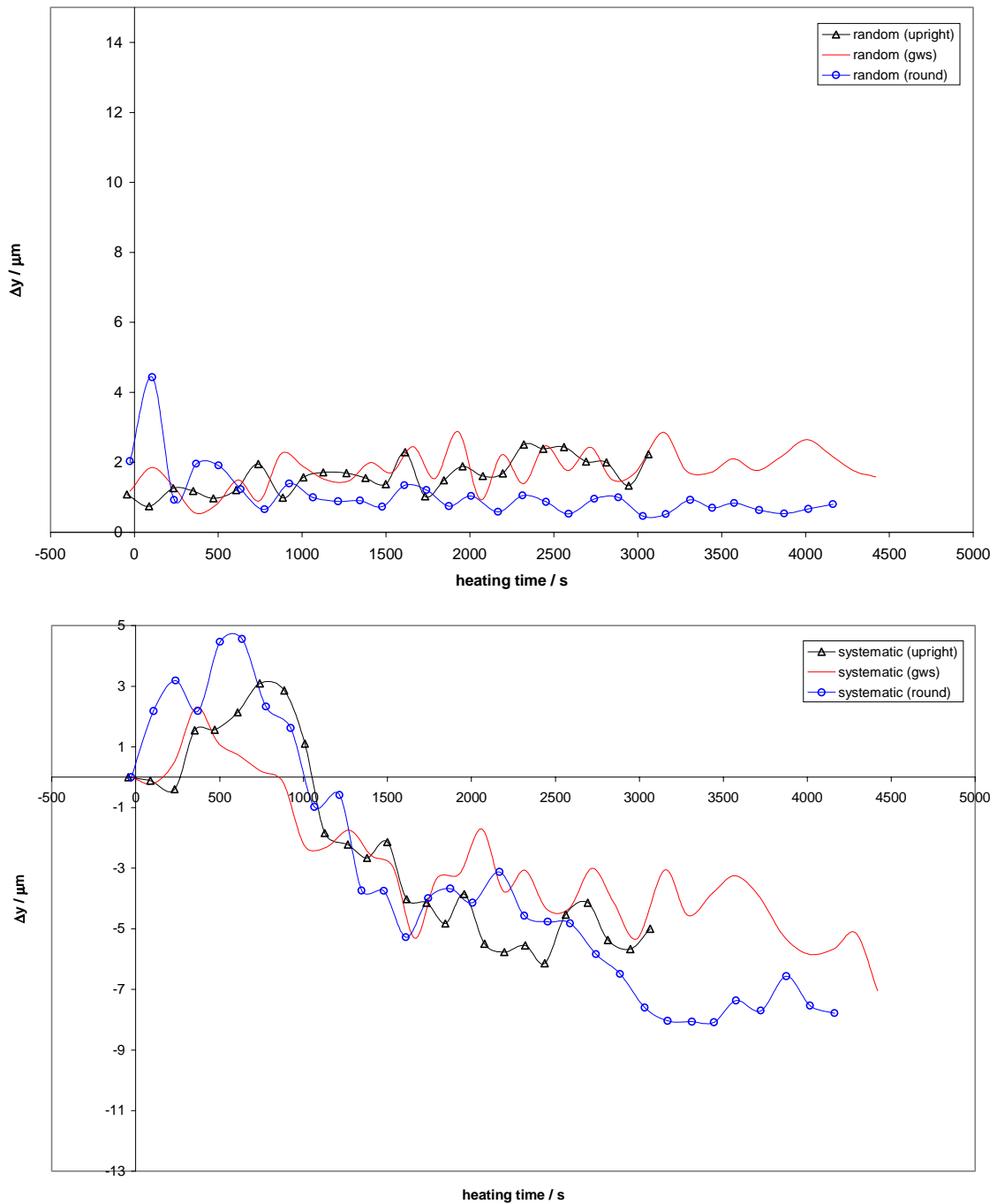


Fig. 23: Random and systematic errors with different shields. Beam passes at the bottom.

In the systematic error plot of the previous figure (as well as in fig.18) the phenomenon of the layering of the air can be observed. During the first 1000 seconds of heating the gradient is positive with the hot air at the bottom (close to the sheet) causing the beam to be deviated upwards. After this period the hot air settles at the top of the shield (although the shield is warmer at the bottom) yielding a negative gradient.

7.7.3 The Magnification (M)

The errors are given relative to the initial magnification (M_0). ΔM is the standard deviation of ten consecutive measurements. The initial random error of the magnification (=without heating) is about ten times higher with the big setup than with the small one ($\approx 3 \cdot 10^{-5}$). Blurring sums up due to the longer path the light travels through (more or less) turbulent air and the numerical aperture ($NA_{\text{big}} = 0.007$) is about ten times lower than with the small setup ($NA_{\text{mini}} = 0.077$).

$$NA = n \sin \theta_0 \approx \frac{D}{2g} \quad (31)$$

where:

n...refractive index of air

θ_0 ...half angle under which the lens frame is "seen" by the object

D...lens diameter

g...distance between mask and lens

In order to achieve a better resolution, there are two measures to be taken: Increase lens diameter and / or use evacuated shields. Another possibility to decrease temperature gradients in shields is to fill them with a gas of higher heat conductivity, e.g. helium. The advantage over using vacuum is that the shield can be inflated at atmospheric pressure relieving the strain on the entrance and exit windows.

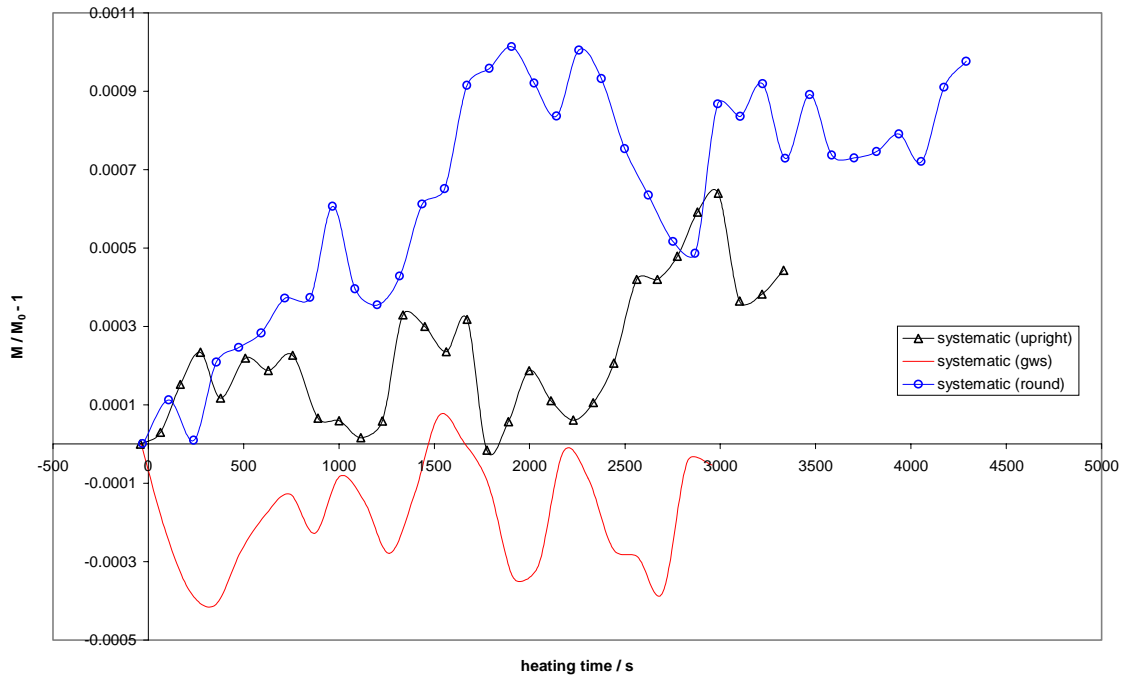
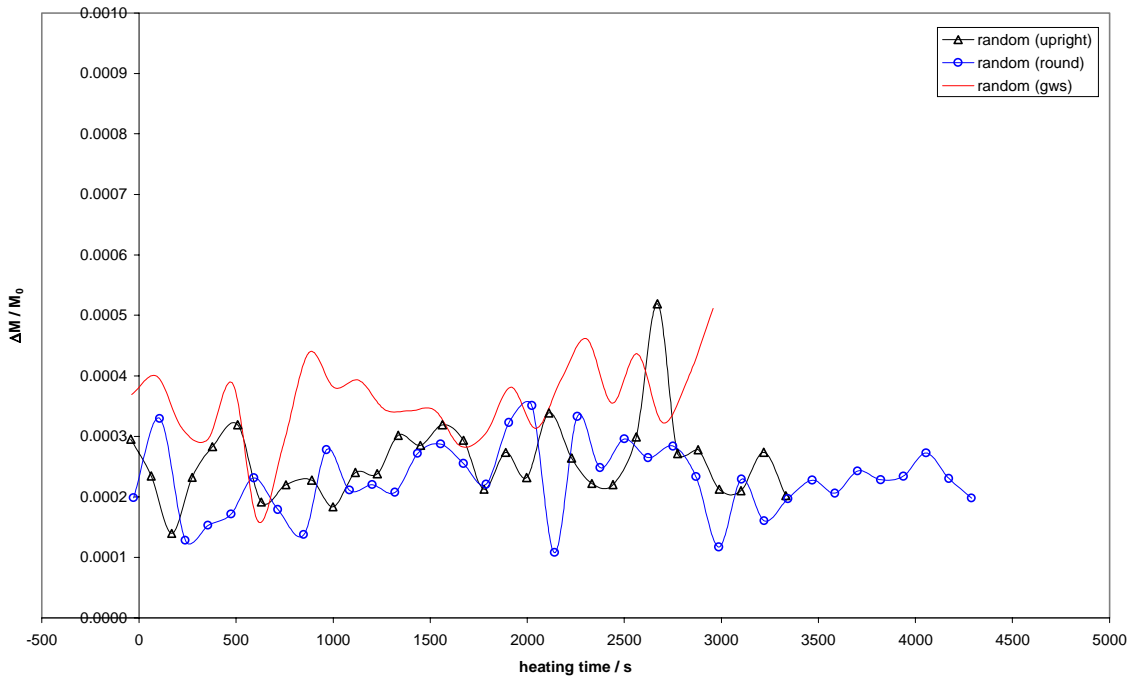


Fig. 24: Random and systematic errors with different shields. Beam passes at the top.

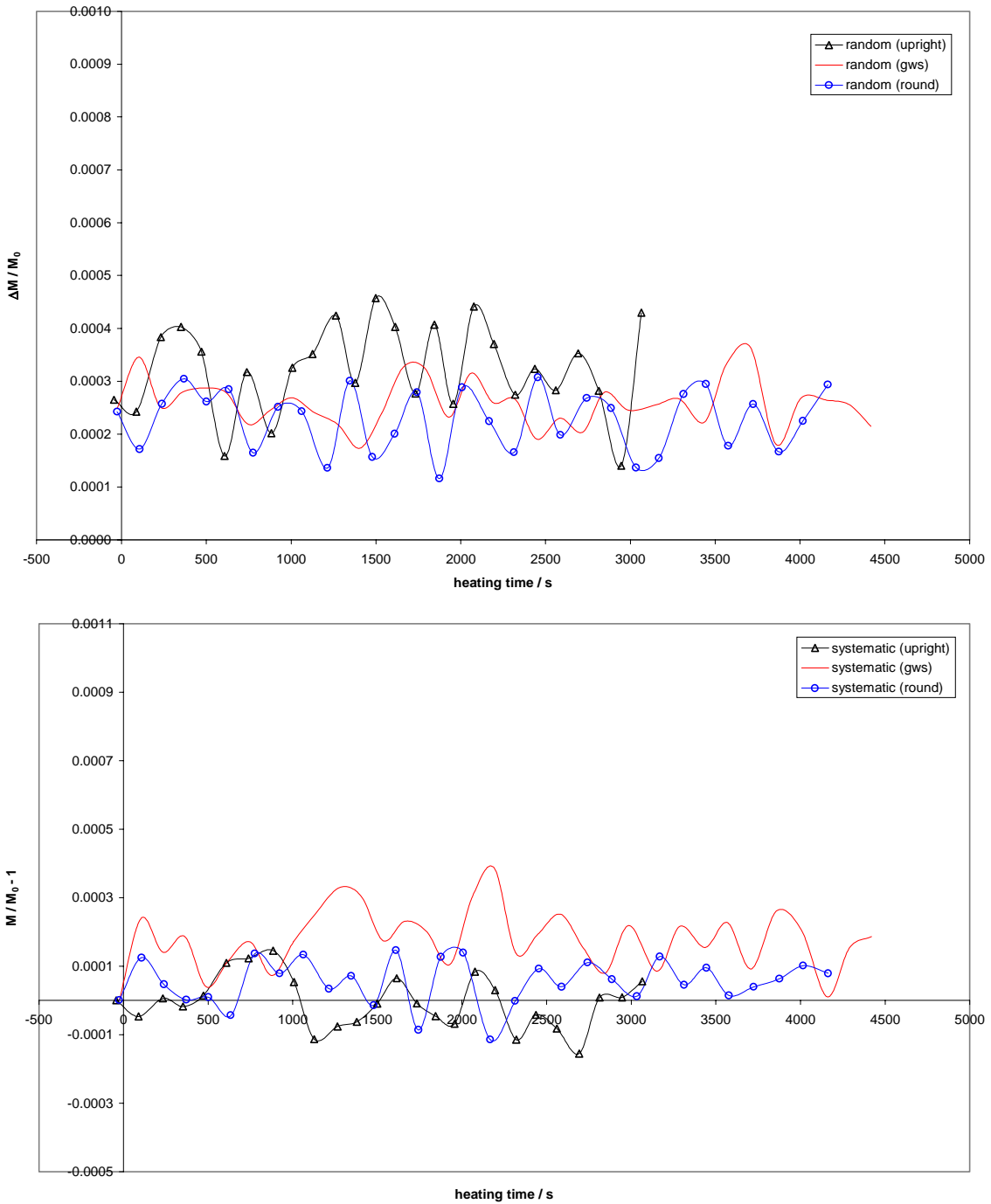


Fig. 25: Random and systematic errors with different shields. Beam passes at the bottom.

When studying the previous plots, one can easily observe that the common round shield gives the smallest random errors but creates large systematic errors. The systematic error in y is smaller when the beam passes at the bottom. The systematic error in x is the greater the closer the beam is to the side shields (see fig.20). Hence, the temperature gradient within the shields is largest at the top and in the vicinity of the side shields. The most

straightforward measure is to remove both, i.e. to use a plane sheet below the beam. The same setup as before has been used in the next chapter.

7.7.4 The Flat Sheet

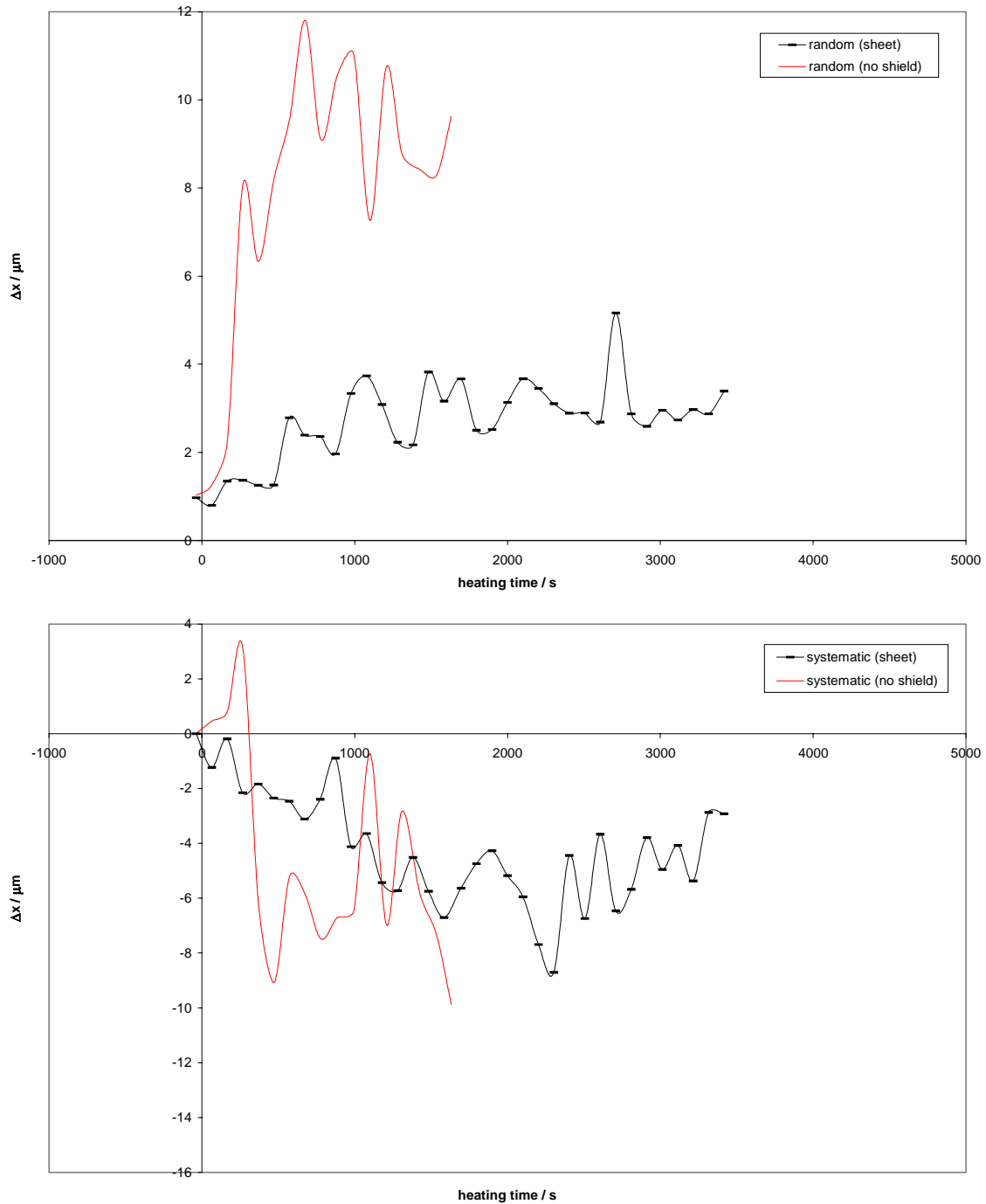


Fig. 26: Random and systematic x errors with the flat aluminum sheet and without shielding. Sheet dimensions: $114.5 \times 59 \times 0.15 \text{ cm}^3$.

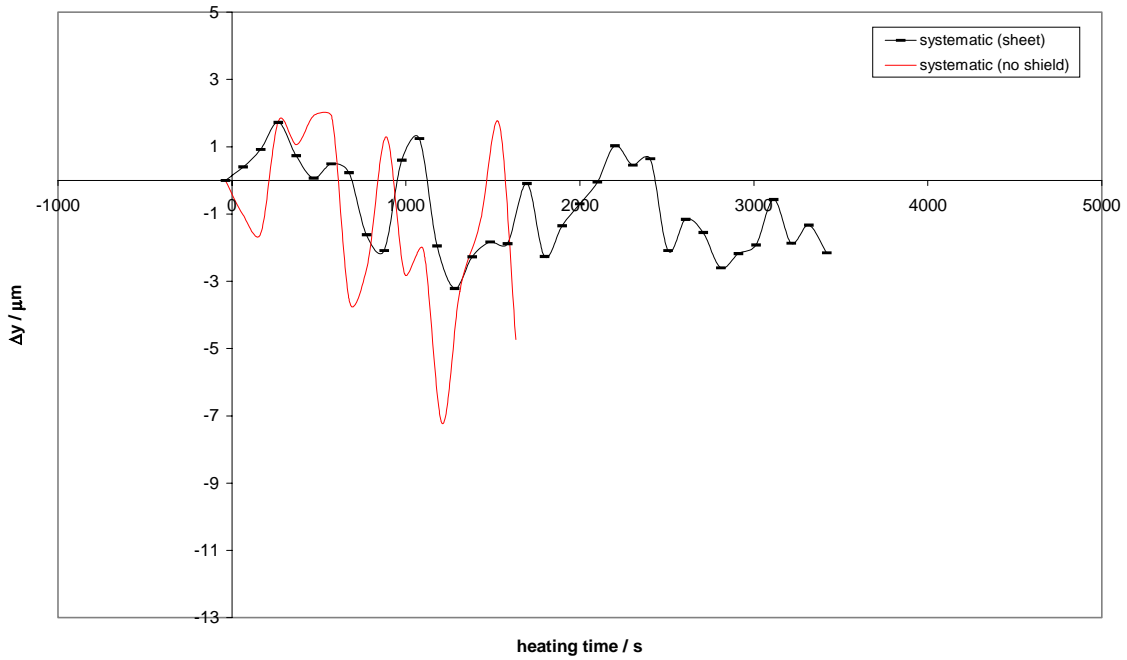
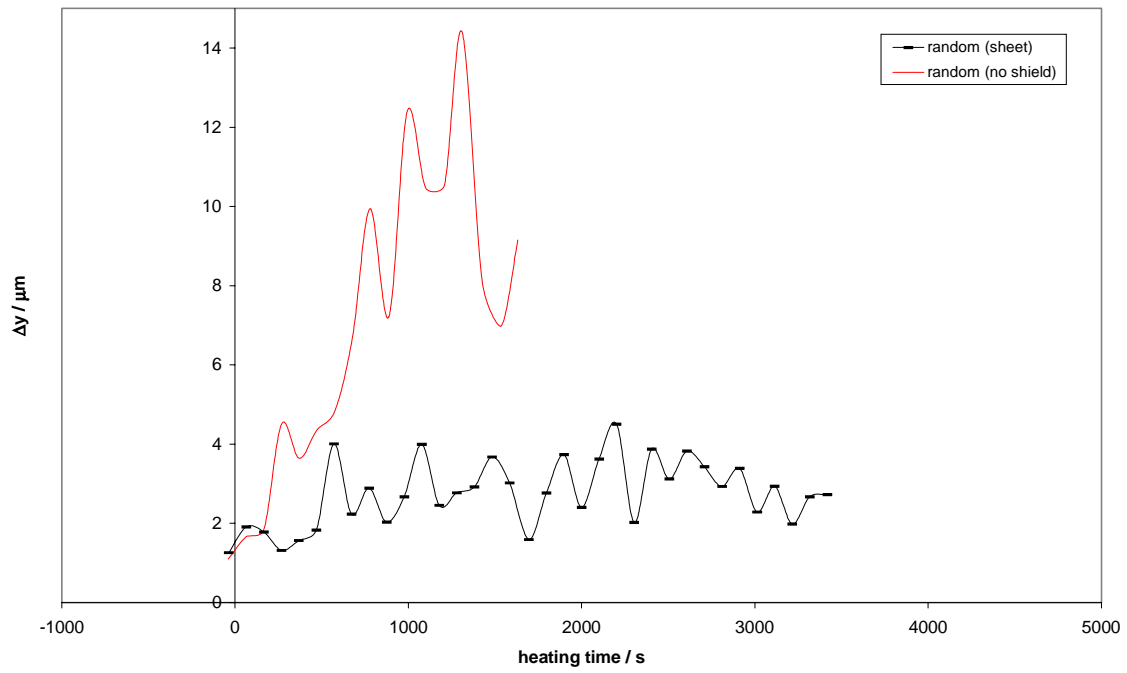


Fig. 27: Random and systematic y errors with the flat aluminum sheet and without shielding.

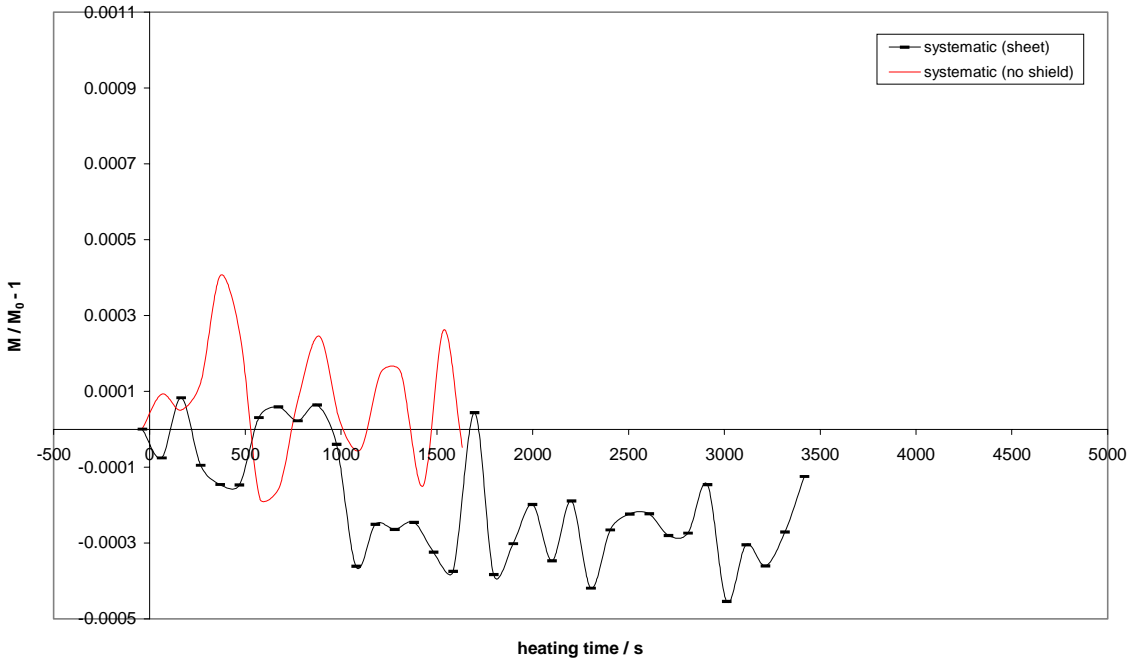
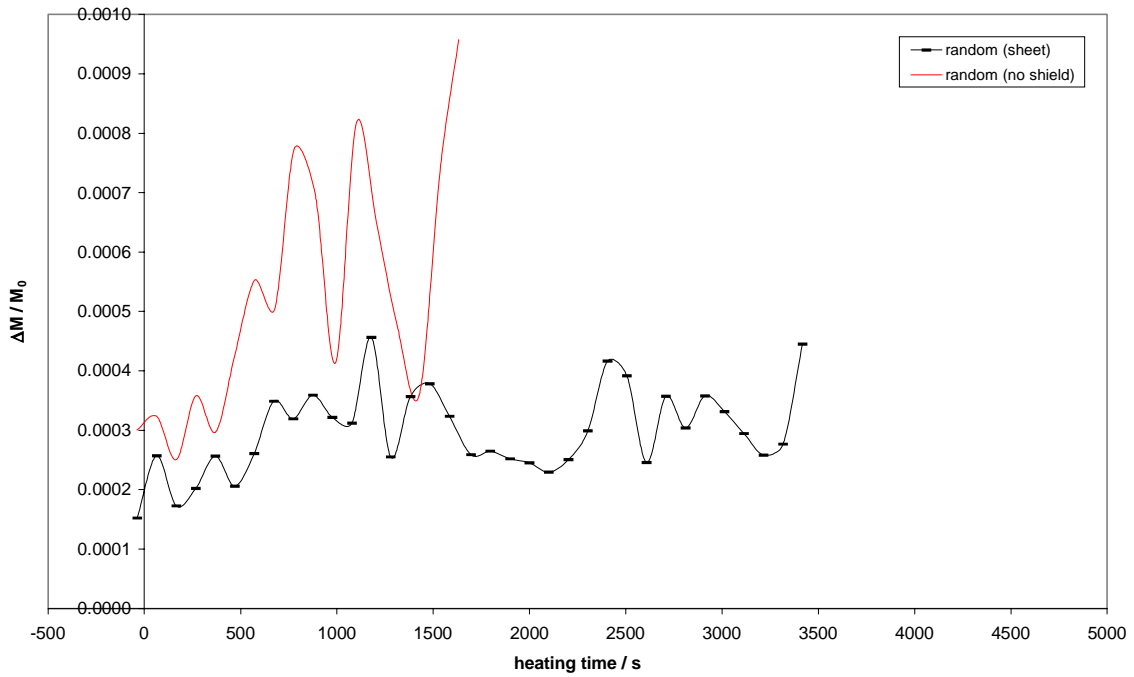


Fig. 28: Random and systematic errors of the magnification (M) with the flat aluminum sheet and without shielding.

With the exception of the x-coordinate, the systematic error is not larger than the random one. The y-coordinate has practically no systematic error. The deviation in the magnification might be due to sagging of the sheet between the supports. This problem can be solved by using T-shape shields, rather than flat ones. The systematic negative x shift in all charts (see esp. fig.26) indicates that the ICARAS – RASNIK system might create this error.

8. ERROR ANALYSIS

If errors of measurement values are relatively small compared to others, they will be neglected in the following equations.

$$\text{Equation 5: } \frac{\Delta p}{p} = \frac{\Delta M_{\infty}}{M_{\infty}}$$

$$\text{Equation 7: } \frac{\Delta c}{c} = \frac{\Delta \text{int ercept}}{\text{int ercept}}$$

$$\text{Equation 16: } \frac{\Delta K}{K} = \frac{\Delta h}{h} + \frac{\Delta(t_b - t_t)}{|t_b - t_t|}$$

$$\text{Equation 25: } \frac{\Delta(\Delta y)}{\Delta y} = \frac{\Delta K}{|K|} + \frac{2(\Delta b + \Delta a) + \Delta l}{|2(b - a) - l|}$$

$$\text{Equation 28: } \frac{\Delta(\Delta y)}{\Delta y} = \frac{\Delta K}{|K|} + \frac{2(\Delta g + \Delta a) + \Delta l}{|2(g - a) - l|} + \frac{\Delta g}{|g - f|}$$

$$\text{Equation 29: } \Delta \bar{n} = \frac{\Delta n_0 \alpha}{(1 + \alpha t)^2} \Delta t$$

9. CONCLUSION

With the method given the effective pixel size was determined with a relative accuracy of $4.7 \cdot 10^{-5}$ and the distance between ccd diode array and protection glass with a relative accuracy of 7.4 %. No significant mask pitch variations (smaller than 0.3 microns over 20 mm) of the 120 microns mask were measured. However, ccd pitch variations of up to $2 \cdot 10^{-3}$ were observed. The ultimate performance revealed an rms of 0.1 μm in the x- and y-coordinates, and a relative random error in the magnification of $3 \cdot 10^{-5}$. Linearity could be shown for the x-, y-, z-, and rot z – coordinates. The values of rot x and rot y could be used as qualitative indicators of rotational movements at best. The minimum required LED current for illuminating the mask was indicated by a failure of the ICARAS system rather than a rise of the random error. Theoretical and measured image displacements caused by a constant air temperature gradient agreed within the error tolerance. The systematic errors created by common shields in a heat dissipating environment gave rise to using plane metal sheets which proved better.

10. FILES INDEX

All data used for plots and tables are stored as files on “Heinz” in the directory c:\Gary. In order to get the original ICARAS files which are stored in the directory c:\Results\Tempresults, one has to add the number “19” before the Excel file name and change the extension into “res”. This rule is only valid for files with date names.

Chapter 3:	970526.xls	Fig.22:	shielding.xls
	970716.xls		970711.xls
	970717.xls		970714.xls
Tab.1:	970516.xls	Fig.23:	shielding.xls
Tab.2:	Report.xls		970709.xls
	970707.xls		970710.xls
	970708.xls	Fig.24:	shielding.xls
Fig.4:	970612.xls		970711.xls
Fig.5:	970612.xls		970714.xls
Fig.6:	970611.xls	Fig.25:	shielding.xls
Fig.7:	970618.xls		970709.xls
Fig.8:	970618.xls		970710.xls
Fig.9:	970618.xls	Fig.26:	shielding.xls
Fig.10:	970613.xls		970714.xls
Fig.14:	970630.xls		970714ns.xls
Fig.15:	970624.xls	Fig.27:	shielding.xls
Fig.16:	970701.xls		970714.xls
Fig.17:	970714ns.xls		970714ns.xls
Fig.18:	970709.xls	Fig.28:	shielding.xls
Fig.19:	970709.xls		970714.xls
Fig.20:	shielding.xls		970714ns.xls
	970711.xls		
	970714.xls		
Fig.21:	shielding.xls		
	970709.xls		
	970710.xls		